Chinese Chemical Letters 35 (2024) 108358

Contents lists available at ScienceDirect

Chinese Chemical Letters

journal homepage: www.elsevier.com/locate/cclet

Synergistic Co-doping effect of CNTs and PVP in $Na_4MnCr(PO_4)_3$ cathode as a strategy for improving the electrochemical performance of SIBs

Ruoyu Chen[a], Denys S. Butenko[b,*], Shilin Li[a], Xinyu Zhang[b], Guangshe Li[c], Igor V. Zatovsky[a,d,*], Wei Han[a,*]

[a] College of Physics, State Key Laboratory of Inorganic Synthesis and Preparative Chemistry, International Center of Future Science, Jilin University, Changchun 130012, China
[b] Academy for Advanced Interdisciplinary Studies, Southern University of Science and Technology, Shenzhen 518055, China
[c] State Key Laboratory of Inorganic Synthesis and Preparative Chemistry, College of Chemistry, Jilin University, Changchun 130012, China
[d] F.D. Ovcharenko Institute of Biocolloidal Chemistry, NAS Ukraine, Kyiv 03142, Ukraine

ARTICLE INFO

Article history:
Received 11 January 2023
Revised 19 February 2023
Accepted 20 March 2023
Available online 21 March 2023

Keywords:
Sodium-ion batteries
$Na_4MnCr(PO_4)_3$
Carbon nanotubes
Polyvinylpyrrolidone
Synergistic effect

ABSTRACT

In order to solve the contradiction between the rapidly growing energy demand and the excessive exploitation of fossil fuels, it is urgent to research and develops more environmentally friendly and efficient energy storage technologies. Therefore, the development of high-performance cathode materials to enhance the energy density of SIB is currently one of the most important topics of scientific research. Advanced high-voltage and low-cost cathode material for SIBs, a composite of carbon-coated $Na_4MnCr(PO_4)_3$ (NASICON-type), polyvinylpyrrolidone (PVP), and modified carbon nanotubes (CNTs) is prepared by sol-gel and freeze-drying method. Due to the high conductivity of CNTs, the conductivity of the composite is significantly improved, and its initial capacity is increased to 114 mAh/g at 0.5 C and 96 mAh/g at 5 C (Mn^{2+}/Mn^{4+} conversion for voltage windows 1.4-4.3 V). Moreover, the multi-electrons transfer of Cr^{3+}/Cr^{4+} and Mn^{2+}/Mn^{4+} can provide a high capacity of 165 mAh/g at 0.1 C and 102 mAh/g at 5 C in the high voltage window of 1.4-4.6 V. Furthermore, PVP can effectively inhibit the Jahn-Teller effect caused by Mn ion, making the composite have more excellent high-rate performance and stability. In addition, GITT, EIS and CV curves were drawn to better reveal the excellent kinetic properties of $Na_4MnCr(PO_4)_3$@C@PVP@CNT cathode, and the mechanism of its performance improvement is deeply studied and discussed. Accordingly, the co-doping of CNTs and PVP is a simple way to high conductivity and fast charging of cathode materials for SIBs.

With the rapid development of today's society, our demand for renewable and clean energy is increasing day by day, so the development and research of large-scale energy storage systems are extremely urgent. So far, LIBs have been widely used in electric vehicles and portable electronic devices [1–6]. However, the cost of lithium has skyrocketed due to the limited and uneven distribution of global lithium resources. The high cost will restrict the development of LIBs. Therefore, recently a hot research topic is the study of a new battery system, which can reduce the load on lithium resources and be used for large-scale energy storage [7–11]. Because of the abundant natural resources, low cost and similar working electrochemical principle to LIBs, sodium-ion batteries (SIBs) have gained widespread attention [12–17]. However, due to the larger ionic radius of sodium ions and the higher intrinsic electrochemical potential of Na^+/Na, the working voltage, energy/power density, cycling stability and other electrochemical characteristics of SIBs are not very ideal compared with LIBs, and these have become the main problems to be solved on the development road of SIBs [18]. Therefore, it is of great significance to develop cathode materials with high working voltage, high specific capacity, high cycle stability and rapid sodium ion diffusion ability to improve the energy density of SIBs.

At present, the cathode materials studied mainly include polyanion compounds, transition metal oxides, Prussian blue derivatives and other materials [18]. Among them, polyanion compounds have been widely concerned because of their excellent

* Corresponding authors.
E-mail addresses: debut98@ukr.net (D.S. Butenko), zvigo@ukr.net (I.V. Zatovsky), whan@jlu.edu.cn (W. Han).

https://doi.org/10.1016/j.cclet.2023.108358
1001-8417/

electrochemical properties due to the "induced effect" of polyanion groups [19]. Among polyanion compounds, phosphate compounds with NASICION-type structure (sodium superionic conductor), such as $Na_3V_2(PO_4)_3$ [20–27], $Na_3V_2(PO_4)_2F_3$ [28–33], $Na_4MnCr(PO_4)_3$ [34–36], $Na_3MnTi(PO_4)_3$ [37], have high working voltage, good thermal stability and safety, the unique three-dimensional open structure, which can be used as a channel for the rapid transport of sodium ions, has been a hot research topic in recent years [38]. And among these cathode materials with NASICION-type structure, $Na_4MnCr(PO_4)_3$ is a kind of electrode material with excellent electrochemical performance. Due to the high cost of vanadium-containing compounds used to synthesize $Na_3V_2(PO_4)_3$, the further application of $Na_3V_2(PO_4)_3$ is limited. By using cheaper Mn^{2+} and Cr^{3+} ions to completely replace the V^{3+} ions of $Na_3V_2(PO_4)_3$, the advanced $Na_4MnCr(PO_4)_3$ cathode materials with low cost and high voltage can be obtained [34]. This material has a higher voltage platform. It can transform Mn^{2+}/Mn^{3+} and Mn^{3+}/Mn^{4+} in the range of 1.4-4.3 V, and can provide a maximum capacity of 114.1 mAh/g at 0.1 C (1 C = 111 mA/g) [34]. There is a Cr^{3+}/Cr^{4+} redox pair in the 4.3-4.6V voltage range. Within the 1.4-4.6 V voltage range, the initial charge and discharge capacity can reach 196/160.5 mAh/g at 0.05 C (1 C = 160 mA/g) [34]. However, due to its low electronic conductivity and the Jahn-Teller effect caused by active Mn^{3+} ions, it shows poor cyclic stability and rate performance in electrochemical tests, which limits its further application. According to Jian Zhang's report [34], $Na_4MnCr(PO_4)_3$ cathode capacity is only 73.5, 60.5, 43.2 and 26.6 mAh/g at 2, 5, 10 and 15 C in 1.4-4.3 V voltage window. $Na_4MnCr(PO_4)_3$ cathode exhibits poor high-rate performance. So many different methods have been tried to improve the performance of materials, such as doping metal cations [39–43], compounding different carbon materials [44–46], and reducing particle size [47,48]. Among them, the composite with carbon material is a common method that can effectively improve the electrical conductivity of the carbon coating and the electrochemical performance of the materials, and has a low cost and simple synthesis method.

Carbon nanotubes (CNTs) and polyvinyl pyrrolidone (PVP) are considered as one of the important materials for improving the electrical conductivity and thermodynamic properties of other materials due to their excellent and unique properties. In fact, CNTs and PVP have been widely used in LIBs and SIBs [46–50]. According to Wei Shen *et al.* [50], they added PVP with different content ratios during the preparation process of $Na_3V_2(PO_4)_3$. Compared with the samples prepared without PVP, the doped samples have a significant improvement in cycle performance and rate performance. On this basis, they chose the best performance of the sample to compound with CNTs, using CNTs as a high conductivity network to further improve the electrochemical performance of $Na_3V_2(PO_4)_3$. The prepared sample shows its excellent rate performance, and the capacity change range is 73-101 mAh/g at a rate of 0.2-70 C [50].

In this work, composites of $Na_4MnCr(PO_4)_3$ cathode material with carbon coating for SIBs and modified CNTs, polyvinylpyrrolidone (PVP), or their combination were prepared through a simple sol-gel method and freeze-drying technology. It was found that the co-doping of CNTs and PVP significantly improves the practically important electrochemical characteristics of $Na_4MnCr(PO_4)_3$, especially the electrical conductivity and stability of the charge/discharge cycle. In particular, the $Na_4MnCr(PO_4)_3$@C@PVP@CNTs material has a high capacity of 114 mAh/g at 0.5 C (voltage windows 1.4-4.3 V), and a long-cycle performance at 5 C is significantly better than other control samples. Furthermore, for the electrochemical window 1.4-4.6 V, the initial capacity of the composite reaches 165 mAh/g at 0.1 C due to the implementation of electrochemical transformations Mn^{2+}/Mn^{4+} and Cr^{3+}/Cr^{4+}. The reasons for the decrease in capacity and long-cycle stability resulting in a high-voltage window are discussed.

To compare the electrochemical properties of $Na_4MnCr(PO_4)_3$ with carbon coating (denoted as NMCP@C hereafter) and its various composite materials (denoted as NMCP@C@CNT NMCP@C@PVP and NMCP@C@PVP@CNTs were prepared (see Experimental section in Supporting information). The general scheme preparation of the NMCP@C@PVP@CNTs sample is shown in Fig. S1 (Supporting information). First, CNTs were acidified to remove impurity phases and increase the functional number of groups on the surface. Then the sol-gel method and lyophilization technology were applied. NMCP@C@PVP@CNTs compound gel obtained by sol-gel method was instantaneously frozen with liquid nitrogen and then freeze-dried. Through the lyophilization technology, the gel was dried by sublimating water, which could not damage the spatial structure inside the compound material, maintain the morphology of the material to the maximum extent, and ensure the uniformity of distribution of CNTs and PVP in the gel. In addition, citric acid and polyvinylpyrrolidone (PVP) were used as carbon sources to form a carbon coating on the surface of the cathode material after calcination at high temperature. XRD patterns of NMCP composites are presented in Fig. 1a. As can be seen, the results of XRD samples for doped CNTs and PVP or CNTs + PVP are similar, and there are only reflexes appurtenant to the rhombohedral structure of NASICON (sp. gr. R-3c). Accordingly, the carbon layer does not affect the crystal structure of $Na_4MnCr(PO_4)_3$ [35,36].

In order to study the microstructure of NMCP series materials, SEM and HRTEM were used. The morphology of all samples is similar: mostly irregular block particles with a size of about 1-5 um (Fig. 1b and Fig. S2 in Supporting information). On the surface of the samples, NMCP@C@PVP@CNT (Fig. 1c) and NMCP@C@CNTs (Fig. S2b) located randomly CNTs can be found, which confirms the successful doping of CNTs. HRTEM images of prepared samples (Fig. 1d and Fig. S2d) clearly show the lattice interplanar distance of $Na_4MnCr(PO_4)_3$. The interplanar distances of about 0.372 and 0.257 nm are in good agreement with the crystal lattice indices (113) and (300) for NMCP (according to card PDF-#97-026-0210), respectively. In addition, a uniform thin layer of carbon with a thickness of about 3-7 nm is observed on the surface of NMCP materials as a result of the carbonization of citric acid and PVP under an inert atmosphere at high temperature. Fig. 1e shows the element mapping analysis of the NMCP@C@PVP@CNTs sample. As shown in the EDX mapping images of Na, Cr, Mn, P, O and C elements, the prepared sample has no additional impurity peaks and the carbon-coated layer was uniformly the surface of NMCP particles.

The I_D/I_G values of NMCP@C@PVP@CNTs and NMCP@C samples (according to Raman spectrum, Fig. 2a) are 0.94 and 1.32, respectively. This indicates that, compared with the NMCP@C sample, the NMCP@C@PVP@CNTs sample has a higher graphitization degree and better electronic conductivity [50]. Moreover, there is an extra peak around 1036 cm^{-1}, which is related to the stretching vibration of the P-O bond [36]. In the FTIR spectrum (Fig. 2b), the presence of the P-O bond of the PO_4 tetrahedron was also detected at about 1058 cm^{-1}. In addition, the stretching vibration of PO_4 units was detected at 1176 cm^{-1}, while the peaks at 670 cm^{-1} and 621 cm^{-1} were caused by the stretching vibration of Cr-O and Mn-O, respectively [51,52]. X-ray photoelectron spectroscopy (XPS) was used to further analyze the valence states of each element on the surface of the prepared samples (Fig. 2c), and the peaks of Na, Mn, Cr, P, O and C can be clearly observed for the all XPS spectrum. The high-resolution XPS spectra of Mn 2p and Cr 2p show the signal of Mn^{2+} and Cr^{3+}, respectively. In the case of the C 1s spectrum, the peak near 284.6 eV corresponds to the sp^2 carbon of the C-C bond, while the other strong peak corresponds to the sp^3 carbon with

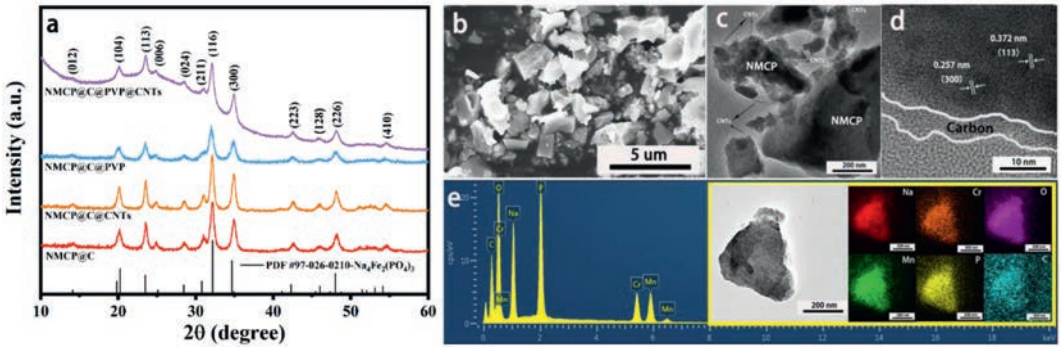

Fig. 1. Characterizations of NMCP@C@PVP@CNTs sample: (a) XRD patterns; (b) SEM image; (c) TEM image; (d) HR-TEM image; (e) EDS element mapping.

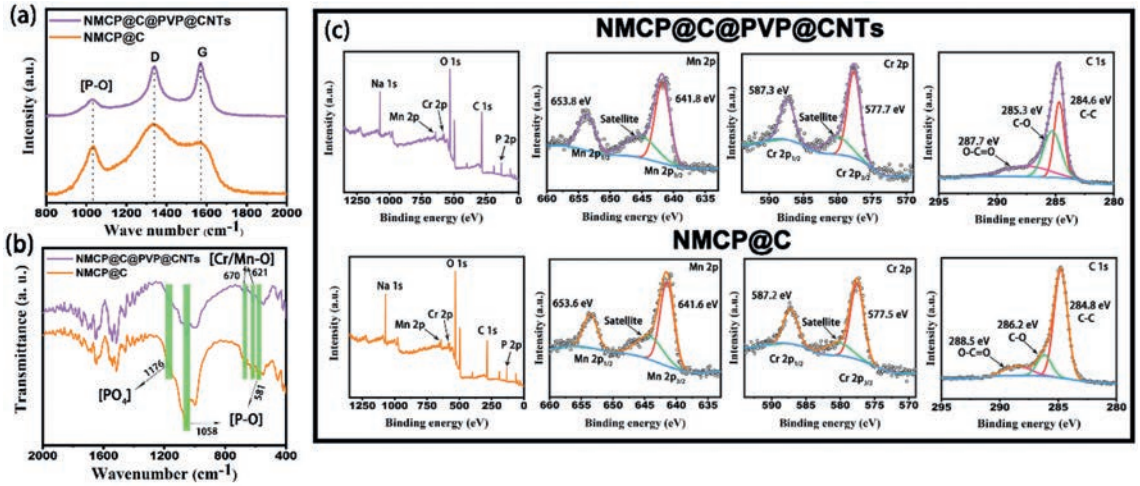

Fig. 2. (a) Raman spectrum; (b) FTIR spectrum of NMCP@C @PVP@CNTs and NMCP@C; (c) Whole XPS spectrum and high-resolution XPS spectra of Mn 2p, Cr 2p, C 1s for NMCP@C@PVP@CNTs and NMCP@C.

several different C-O bond configurations, namely the C-O bond at about 285.3 eV and O-C=O bond at about 287.7 eV. In addition, by comparing the XPS spectra of the two samples, it can be seen that the chemical bond of elements in the samples doped with CNTs and PVP remains unchanged.

The result of thermogravimetric analysis (TGA) revealed that the weight loss of the NMCP series samples during the heating process is used to evaluate the carbon content in the prepared samples (see details in Supporting information).

The electrochemical characteristics of all prepared samples were measured in semi-elements of sodium ions by assembling push-button elements CR2032. The electrodes were tested on two different voltage windows, 1.4-4.3 V and 1.4-4.6 V, respectively. Fig. 3a shows the CV curve of the NMCP@C@PVP@CNTs electrode with a voltage window of 1.4-4.3 V (for other samples, see Fig. S4 in Supporting information). It can be clearly seen that there are two pairs of redox peaks at 3.46/3.74 V and 4.14/4.26 V, which correspond to the redox reactions of $Na_4MnCr(PO_4)_3/Na_3MnCr(PO_4)_3$ and $Na_3MnCr(PO_4)_3/Na_2MnCr(PO_4)_3$, respectively [36]. In addition, the highly overlapping CV curves also reflect the high reversibility of the redox reactions of Mn^{2+}/Mn^{3+} and Mn^{3+}/Mn^{4+}, which means the high reversibility of the deintercalation behavior of sodium ions in NMCP@C@PVP@CNTs material. Fig. 3b shows the GITT test results of the NMCP@C@PVP@CNTs electrode in the range of 1.4-4.3 V (the typical charge and discharge GITT curve in the second circle); for NMCP@C@CNTs, NMCP@C@PVP and NMCP@C are shown in Figs. S5 and S6a (Supporting information), respectively. The battery was charged and discharged for 30 min at 0.1 C current density (Fig. S7 in Supporting information), after which it was rested for 2 h to achieve voltage balance. According to the calculation for NMCP@C@PVP@CNTs, the sodium ion diffusion coefficient D_{Na^+} is approximately between 10^{-12} cm^2/s and 10^{-10} cm^2/s. After the GITT test of the NMCP@C electrode under the same conditions, the calculated value of D_{Na^+} is about 10^{-15}-10^{-10} cm^2/s. It can be seen that the co-doping of PVP and CNTs can improve the sodium ion diffusion coefficient D_{Na^+}.

The results of electrochemical charge/discharge tests at different current densities for NMCP composites in the potential window of 1.4-4.3 V *vs.* Na^+/Na are shown in Fig. 3 and Fig. S8 (Supporting information). The charge/discharge curves of the first five cycles for the NMCP@C@PVP@CNTs at 0.5 C (Fig. 3c, 1 C = 110 mA/g) clearly demonstrate the existence of two electrochemical platforms at 3.51/3.67 V and 4.15/4.26 V (correspond to the redox process of Mn^{2+}/Mn^{3+} and Mn^{3+}/Mn^{4+}, as a result, two sodium ions are deintercalated), respectively, that is in good agreement with CV profiles (Fig. 3a). The theoretical capacity of double electron transfer of NMCP@C based on $Mn^{2+}/Mn^{3+}/Mn^{4+}$ is 110.8 mAh/g [34–36]. However, in the cyclic performance at 0.5 C (Fig. 3d), it is found that the capacity of NMCP@C@CNTs (119 mAh/g, 1st cycle) and NMCP@C@PVP@CNTs (114 mAh/g, 2nd and 3rd cycle) is slightly higher than the theoretical value due to the small amount of Cr^{3+}/Cr^{4+} involved in the reaction to provide the capacity [34]. In general, the initial specific capacity of NMCP@C, NMCP@C@PVP, NMCP@C@CNTs and NMCP@C@PVP@CNTs is 95, 93, 119 and 109 mAh/g, respectively. This indicates that a revision phase conversion between $Na_4MnCr(PO_4)_3/Na_3MnCr(PO_4)_3$ is carried up to 4.3 V. During the cycling performance at 0.5 C (Fig. 3d), the specific capacity for all samples is gradually reduced, and af-

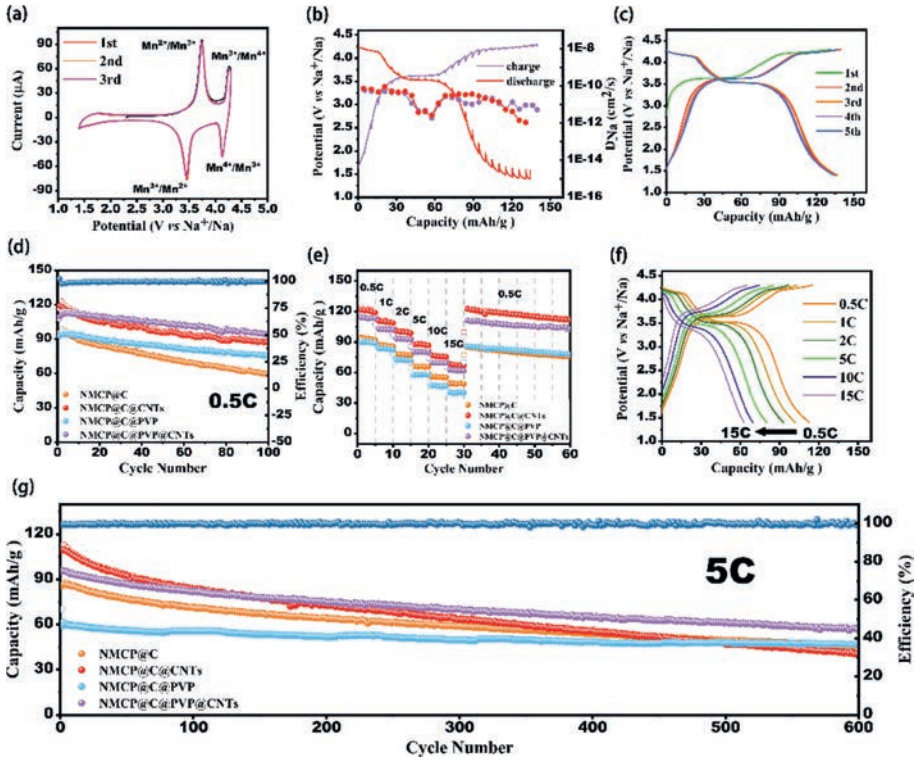

Fig. 3. Electrochemical performance of NMCP composites: (a) Cyclic voltammetry (CV) profiles of NMCP@C@PVP@CNTs at 0.2 mV/s. (b) Galvanostatic intermittent titration technique (GITT) profiles and the corresponding calculated Na^+ diffusion coefficients (D_{Na^+}) of NMCP@C@PVP@CNTs during charge/discharge processes at 0.1 C. (c) Charging/discharging profiles of NMCP@C@PVP@CNTs at 0.5 C. (d) cycling stability of NMCP series samples at 0.5 C. (e) Rate capability of NMCP series samples at different rates; (f) charging/discharging profiles of NMCP@C@PVP@CNTs at different rates. (g) Long-term cycle performance of NMCP series samples under a high rate of 5 C.

ter 100th cycle the capacity is retention at the level 62.5%, 74.3%, 81.5% and 86.2% for NMCP@C, NMCP@C@CNTs, NMCP@C@PVP and NMCP@C@PVP@CNTs, respectively (Table S1 in Supporting information). The performance tests from 0.5 C to 15 C were conducted to study the rate performance of NMCP series electrodes at various current densities (Fig. 3e). It can see that the rate performances of NMCP@C@CNTs and NMCP@C@PVP@CNTs samples were better than of NMCP@C and NMCP@C@PVP. So, the specific capacities of NMCP@C@PVP@CNTs at 0.5, 1, 2, 5, 10 and 15 C are 114, 103, 93, 80, 70 and 63 mAh/g, respectively, and after returning to 0.5 C, the capacity can reach 111 mAh/g. Therefore, doping CNT allows for increasing the capacity and rate performance of NMCP@C material due to the excellent electrical conductivity of CNTs. Fig. 3f and Fig. S8 display the charge-discharge curves of NMCP@C@PVP@CNTs and NMCP@C at different rates. At a low current of 0.5 C, there are two continuous flat voltage platforms at 3.52/3.63 V and 4.18/4.26 V, but when the current increases to 5 C, the platform at 3.52/3.63 V has a slight potential shift, and the voltage plateau at 4.18/4.26 V began to decrease. Increasing the current to 15 C causes the potential of the low-potential voltage plateau to shift to 3.38/3.77 V, and the high-potential platform almost disappeared. Although the charge-discharge curves of NMCP@C and NMCP@C@PVP@CNT are similar, the capacity of NMCP@C is significantly lower than NMCP@C@PVP@CNT at all rates. This indicates that the co-doping of PVP and CNTs is helpful to improve the stability of the crystal structure of NMCP. In addition, the long-term cycle performance of NMCP samples were tested at 5 C (Fig. 3g). The initial capacity of the electrodes is in the range from 109 mAh/g to 70 mAh/g at the rate of 5 C (maximum for NMCP@C@CNTs and minimum for NMCP@C@PVP, more detail in Table S2 in Supporting information). After 600 cycles the specific capacity retention of NMCP@C, NMCP@C@PVP, NMCP@C@CNTs and NMCP@C@PVP@CNTs is 52.9%, 67.1%, 37.5% and 59.3%, respectively, and the capacity of NMCP@C@PVP@CNT is 57 mAh/g, which is higher than in all other samples (Table S2). It is noteworthy that although the doping of CNTs helps to increase the conductivity of NMCP and thus increase the capacity, however, CNTs with one-dimensional structure have little contribution to the cyclic stability of NMCP materials, so the long-term cycle performance of NMCP@C@CNTs samples is the worst. In fact, the decrease in cyclic stability of NMCP materials is generally attributed to the Jahn-Teller effect caused by active Mn^{3+} ions, which leads to the distortion of the material lattice and the loss of manganese ions from the electrode to the electrolyte [34–36]. Due to the addition of CNTs during the charge-discharge process, additional sodium ion diffusion channels are added inside the material, so the conductivity and initial capacity of NMCP@C@CNTs and NMCP@C@PVP@CNTs cathode are significantly improved. However, at the same time, the repeated ionized short-chain CNTs aggravated the Jahn-Teller effect [53], and the increase of these sodium channels also promoted the dissolution of the active Mn^{3+} ions that caused the Jahn-Teller effect, resulting in a significant decrease in the cyclic stability of NMCP@C@CNTs cathode. Interestingly, the addition of PVP significantly improved the cycle stability of the NMCP cathode. From the cycling performance at 0.5 C and the long cycling performance at 5 C, the cycling stability of NMCP@C@PVP@CNTs cathode was significantly improved while maintaining high electrochemical capacity. Moreover, the NMCP@C@PVP cathode has the most stable long-term cycling performance. On the one hand, PVP is carbonized due to incomplete combustion during the calcination at high temperature in an inert atmosphere, forming an additional conductive carbon coating with rich defects to cover the surface of the material particles, thus significantly improving the Na^+ diffusion rate and conductivity, and the doping of PVP can also effectively reduce the side reaction between electrode/electrolyte interface, thus forming a thinner CEI layer and improving the cycle

stability [47-49,54,55]. On the other hand, PVP, as a non-ionic surfactant, forms micelles in an aqueous solution and disperses particles, which can effectively adjust the shape and size of particles, so the sample doped with PVP can have a more uniform and small size. During the cycle, there is a certain space between PVP-doped material particles to release the lattice stress caused by Jahn-Teller distortion, thus maintaining its structural stability [56]. It is apparent that because of the synergistic effect of PVP and CNTs, the capacity and cycle stability of the NMCP@C@PVP@CNTs sample have been significantly improved at different current densities. In addition, electrochemical impedance spectroscopy (EIS) and CV tests on the electrode at various scan rates from 1.4 V to 4.3 V were performed for the determination of the kinetics of the electrode processes in the prepared samples (details see Supporting information). A comparison of the discharge capacity of the NASICON-type is given in Table S6 (Supporting information). As can be seen from the data presented, the obtained values for prepared CNTs- and PVP-doped $Na_4MnCr(PO_4)_3$/C composite are significantly higher or approximately equal to those previously reported.

Since in NMCP, the redox reaction of Cr^{3+}/Cr^{4+} can also take place due to a wider voltage window, additional electrochemical tests were carried out for NMCP@C@PVP@CNTs and NMCP@C in the voltage range of 1.4-4.6 V (Fig. S11 in Supporting information). It should be noted that the expansion of the voltage window, on the one hand, leads to a significant increase in capacitive characteristics due to the additional one, but on the other hand, cyclic stability worsens (details in Supporting information).

In addition, we use multilayer $V_4C_3T_x$ MXene instead of sodium metal and NMCP@C@PVP@CNTs as the anode and cathode, respectively, are assembled into coin cells to study the full battery performance (see details in Supporting information).

In summary, we adopted sol-gel and freeze-drying methods for the synthesis of NMCP composites achieved by carbon-coated, PVP, and modified CNTs. It was found that co-doping of CNTs and PVP creates a synergistic effect to improve practically important electrochemical characteristics of the NMCP@C cathode material in SIBs, namely: promoting high-rate capability (114 mAh/g at 0.5 C and 96 mAh/g at 5 C), well supports a long-life cycle (600 cycles at 5 C), improves kinetic parameters and sodium diffusion coefficients (D_{Na^+} about 2.3×10^{-12} cm^2/s), electrical conductivity increases significantly (R_p is 103 Ω). The specified results are determined for voltage windows within 1.4-4.3 V. Expanding the voltage window to 1.4-4.6 V also allows, due to Cr^{3+}/Cr^{4+} transformations, to increase the output capacity up to a value of 165 mAh/g at 0.1 C, and this result is the best. However, at high current densities partially invalidates these results due to electrolyte decomposition. Accordingly, for the effective industrial implementation of NMCP cathodes or similar materials, the creation of new electrolytes.

Declaration of competing interest

The authors declare that they have no known competing financial interests or personal relationships that could have appeared to influence the work reported in this paper.

Acknowledgment

This work was supported by the National Natural Science Foundation of China (NSFC, Nos. 21571080, 62174152 and 12204219).

Supplementary materials

Supplementary material associated with this article can be found, in the online version, at doi:10.1016/j.cclet.2023.108358.

References

[1] M. Armand, J.M. Tarascon, Nature 451 (2008) 652–657.
[2] J.B. Goodenough, Y. Kim, Chem. Mater. 22 (2010) 587–603.
[3] C.X. Zu, H. Li, Energy Environ. Sci. 4 (2011) 2614–2624.
[4] P. Senguttuvan, G. Rousse, V. Seznec, J.M. Tarascon, M.R. Palacín, Chem. Mater. 23 (2011) 4109–4111.
[5] X. Zhou, L.J. Wan, Y.G. Guo, Adv. Mater. 25 (2013) 2152–2157.
[6] J. Xu, Y. Xu, C. Lai, et al., Sci. China Chem. 64 (2021) 1267–1282.
[7] H. Li, H. Zhou, Chem. Commun. 48 (2012) 1201–1217.
[8] F.T. Wagner, B. Lakshmanan, M.F. Mathias, J. Phys. Chem. Lett. 1 (2010) 2204–2219.
[9] H. Li, Z. Wang, L. Chen, X. Huang, Adv. Mater. 21 (2009) 4593–4607.
[10] A. Kraytsberg, Y. Ein-Eli, Nano Energy 2 (2013) 468–480.
[11] I. Shterenberg, M. Salama, Y. Gofer, E. Levi, D. Aurbach, MRS Bull. 39 (2014) 453–460.
[12] P. Alotto, M. Guarnieri, F. Moro, Renew. Sustainable Energy Rev. 29 (2014) 325–335.
[13] Y. Man, J. Sun, X. Zhao, et al., J. Colloid Interf. Sci. 635 (2023) 417–426.
[14] E. Gu, S. Liu, Z. Zhang, et al., J. Alloys Compd. 767 (2018) 131–140.
[15] H. Chen, M. Li, C. Li, et al., Chin. Chem. Lett. 33 (2022) 141–152.
[16] G. Xu, Q. Wang, Y. Su, et al., J. Acta Phys. Chim. Sin. 38 (2022) 2009073.
[17] S. Yang, B. Wang, Q. Lv, et al., Chin. Chem. Lett. 34 (2023) 107783.
[18] V. Palomares, P. Serras, I. Villaluenga, et al., Energy Environ. Sci. 5 (2012) 5884–5901.
[19] D. Bin, F. Wang, A.G. Tamirat, et al., Adv. Energy Mater. 8 (2018) 1703008.
[20] J. Kang, V.Mathew S.Baek, et al., J. Mater. Chem. 22 (2012) 20857–20860.
[21] H. Xiong, G. Sun, Z. Liu, et al., Angew. Chem. Int. Ed. 60 (2021) 10334–10341.
[22] W. Shen, C. Wang, H. Liu, W. Yang, Chem. Eur. J. 19 (2013) 14712–14718.
[23] W. Duan, Z. Zhu, H. Li, et al., J. Mater. Chem. A 2 (2014) 8668–8675.
[24] S.J. Lim, D.W. Han, D.H. Nam, et al., J. Mater. Chem. A 2 (2014) 19623–19632.
[25] M.J. Aragón, P. Lavela, G.F. Ortiz, J.L. Tirado, ChemElectroChem 2 (2015) 995–1002.
[26] J. Yang, D.W. Han, M.R. Jo, et al., J. Mater. Chem. A 3 (2015) 1005–1009.
[27] H. Xiong, R. Qian, Z. Liu, et al., Adv. Sci. 8 (2021) 2004943.
[28] J.M. Le Meins, M.P. Crosnier-Lopez, A. Hemon-Ribaud, G. Courbion, J. Solid State Chem. 148 (1999) 260–277.
[29] T. Jiang, G. Chen, A. Li, C. Wang, Y. Wei, J. Alloys Compd. 478 (2009) 604–607.
[30] R.K.B. Gover, A. Bryan, P. Burns, J. Barker, Solid State Ionics 177 (2006) 1495–1500.
[31] M. Bianchini, N. Brisset, F. Fauth, et al., Chem. Mater. 26 (2014) 4238–4247.
[32] R.A. Shakoor, D.H. Seo, H. Kim, et al., J. Mater. Chem. 22 (2012) 20535–20541.
[33] Q. Liu, X. Meng, Z. Wei, et al., ACS Appl. Mater. Interfaces 8 (2016) 31709–31715.
[34] J. Zhang, Y. Liu, X. Zhao, et al., Adv. Mater. 32 (2020) 1906348.
[35] Y. Zhao, X. Gao, H. Gao, A. Dolocan, J.B. Goodenough, Nano Lett. 21 (2021) 2281–2287.
[36] W. Zhang, H. Li, Z. Zhang, et al., Small 16 (2020) 2001524.
[37] H. Gao, Y. Li, K. Park, J.B. Goodenough, Chem. Mater. 28 (2016) 6553–6559.
[38] Y. Fang, J. Zhang, L. Xiao, et al., Adv. Sci. 4 (2017) 1600392.
[39] Y. Chen, Y. Xu, X. Sun, C. Wang, J. Power Sources 375 (2018) 82–92.
[40] H. Li, X. Yu, Y. Bai, et al., J. Mater. Chem. A 3 (2015) 9578–9586.
[41] H. Li, Y. Bai, F. Wu, Q. Ni, C. Wu, ACS Appl. Mater. Interfaces 8 (2016) 27779–27787.
[42] F. Lalère, V. Seznec, M. Courty, et al., J. Mater. Chem. A 3 (2015) 16198–16205.
[43] H. Li, H. Tang, C. Ma, et al., Chem. Mater. 30 (2018) 2498–2505.
[44] H. Li, T. Jin, X. Chen, et al., Adv. Energy Mater. 8 (2018) 1801418.
[45] F. Li, Y.E. Zhu, J. Sheng, et al., J. Mater. Chem. A 5 (2017) 25276–25281.
[46] L. Chen, Z. Zhong, S. Ren, et al., Energy Technol. 8 (2020) 1901080.
[47] L. Chen, B. Yan, J. Xu, et al., ACS Appl. Mater. Interfaces 7 (2015) 13934–13943.
[48] Y. Hu, L. Wu, G. Liao, et al., Ceram. Int. 44 (2018) 17577–17584.
[49] W. Shen, C. Wang, Q. Xu, et al., Adv. Energy Mater. 5 (2015) 1400982.
[50] W. Shen, H. Li, Z. Guo, et al., ACS Appl. Mater. Interfaces 8 (2016) 15341–15351.
[51] D. Wang, Z. Wei, Y. Lin, et al., J. Mater. Chem. A 7 (2019) 20604–20613.
[52] Y. Ruan, K. Wang, S. Song, J. Liu, X. Han, Ionics 23 (2017) 1097–1105.
[53] P. Szakács, D. Kocsis, P.R. Surján, J. Chem. Phys. 132 (2010) 034309.
[54] Y. Lang, X. Sun, G. Xue, et al., Ionics 28 (2022) 5025–5038.
[55] J.M. Kim, Y. Xu, M.H. Engelhard, et al., ACS Appl. Mater. Interfaces 14 (2022) 17405–17414.
[56] H.B. Lin, Y.M. Zhang, J.N. Hu, et al., J. Power Sources 257 (2014) 37–44.